ELSEVIER

Journal of Hazardous Materials A137 (2006) 654–665

Journal of Hazardous Materials

www.elsevier.com/locate/jhazmat

CFD analysis of gas explosions vented through relief pipes

G. Ferrara [a], A. Di Benedetto [b,*], E. Salzano [b], G. Russo [a]

[a] *Dipartimento di Ingegneria Chimica, Università "Federico II", P.le Tecchio 80, Napoli, Italia*
[b] *Istituto di Ricerche sulla Combustione, CNR, Via Diocleziano 328, 80124 Napoli, Italia*

Received 7 July 2005; received in revised form 7 March 2006; accepted 8 March 2006
Available online 3 May 2006

Abstract

Vent devices for gas and dust explosions are often ducted to safe locations by means of relief pipes. However, the presence of the duct increases the severity of explosion if compared to simply vented vessels (i.e. compared to cases where no duct is present). Besides, the identification of the key phenomena controlling the violence of explosion has not yet been gained. Multidimensional models coupling, mass, momentum and energy conservation equations can be valuable tools for the analysis of such complex explosion phenomena. In this work, gas explosions vented through ducts have been modelled by a two-dimensional (2D) axi-symmetric computational fluid dynamic (CFD) model based on the unsteady Reynolds Averaged Navier Stokes (RANS) approach in which the laminar, flamelet and distributed combustion models have been implemented. Numerical test have been carried out by varying ignition position, duct diameter and length. Results have evidenced that the severity of ducted explosions is mainly driven by the vigorous secondary explosion occurring in the duct (burn-up) rather than by the duct flow resistance or acoustic enhancement. Moreover, it has been found out that the burn-up affects explosion severity due to the reduction of venting rate rather than to the burning rate enhancement through turbulization.

Keywords: Ducted venting; Explosion relief; Gas explosion; CFD

1. Introduction

Vent devices for gas and dust explosions are often ducted to safe locations by means of relief pipes, for the discharge of hot combustion products – even toxic – or blast waves [1,2]. Relief pipes are specifically required when the hot jet flowing violently from the vent area has to be avoided, e.g. within buildings. On the other hand, the presence of a duct is likely to increase the severity of the explosion with respect to simply vented vessels [2–5].

In the last two decades a number of works have addressed the issue of gas explosions vented through relief pipes [4–9]. Several phenomena were identified as affecting the increase of the overpressure with respect to simply vented vessels such as secondary explosion in the duct (burn-up), frictional drag and inertia of the gas column in the duct, acoustic and Helmholtz oscillations.

Acoustic oscillations are deemed to be involved in the generation of later strong pressure peaks in simply vented vessels [10]. Kordylevski and Wach [7] detected acoustic oscillations in the pressure records of their experiments on small-scale ducted vent explosions suggesting this phenomenon could be somehow responsible for the unusual pressure rise in the vessel. Actually the link was quite loose as they observed stronger pressure rises (with respect to simply vented vessels) also in the absence of oscillatory behaviour. Moreover, Ponizy and Leyer [5] reported an increased violence of the duct-vented explosion on a small scale with stoichiometric propane–air mixtures which does not constitute a suitable condition for acoustic enhancement of explosion [11]. Helmholtz oscillations in small explosion chambers fitted to venting ducts were observed early by Cubbage and Marshall [12]. Also, McCann et al. [13] clearly detected Helmholtz oscillations in the final stages of explosions in small-scale vessels fitted to duct of different lengths. They pointed out that such oscillations could play an important role in triggering Taylor instability. Nevertheless, this effect cannot be considered necessary condition for the increase of the explosion violence,

Abbreviations: BML, Bray Moss Libby (model); CFD, computational fluid dynamic; CFL, Courant–Friedrich–Levy (relaxation factor); RANS, Reynolds Averaged Navier Stokes (equations); 2D, two dimensional

* Corresponding author. Tel.: +39 0817682947; fax: +39 0817622915.
E-mail address: dibenede@irc.cnr.it (A. Di Benedetto).

0304-3894/$ – see front matter © 2006 Elsevier B.V. All rights reserved.
doi:10.1016/j.jhazmat.2006.03.037

Nomenclature

A	area (m^2)
c	progress variable
c_1	constant (see Table 1)
c_2	constant (see Table 1)
C_L	constant (=0.5)
D_t	duct diameter (m)
e	internal energy ($J\,kg^{-1}$)
f	empirical function in Abu-Orf and Cant [33]
F	friction factor for the flow in the duct
g	constant (=1.5)
GM	geometrical mean
I_o	mean stretch factor
k	turbulent kinetic energy ($m^2\,s^{-2}$)
K	pressure loss coefficient
Ka	Karlovitz number
l_L	laminar flame thickness (m)
l_T	integral length scale of turbulence (m)
L_t	length of duct (m)
L_y	flamelet wrinkling length scale (m)
$\dot{m}$	mass flow rate ($kg\,s^{-1}$)
P	pressure (bar g)
R^2	regression factor
S_L	laminar burning velocity ($m\,s^{-1}$)
t	time (s)
T	temperature (K)
u	gas velocity ($m\,s^{-1}$)
u'	root mean square velocity ($m\,s^{-1}$)
u_F	flame speed with respect to a fixed observer ($m\,s^{-1}$)
V	volume (m^3)
x	space coordinate (m)
Y	propane mass or molar fraction

Greek symbols

α_I	inertial relaxation factor
α	constant (see Table 1)
β	constant (see Table 1)
χ	flame area enhancement factor due to turbulent wrinkling
Δ	difference across different sections of the rig
ε	dissipation rate of turbulent kinetic energy ($m^2\,s^{-3}$)
φ	analytical function determined in Molkov [19]
ν	kinematic viscosity ($m^2\,s^{-1}$)
ρ	density ($kg\,m^{-3}$)
σ	variance
σ_y	constant (=0.5)
Σ	flame area to volume ratio (m^{-1})
τ	heat release factor
$\dot{\omega}$	reaction rate ($kg\,s^{-1}\,m^{-3}$)
ξ	constant (Eq. (11))

Subscripts and superscripts

b	burned
cell	computational cell value
exp	experimental
F	flame
in	tube entrance
L	laminar
max	maximum value
o	reference conditions
out	referred to the exit section of the duct to the atmosphere
t	tube
T	turbulent
u	unburned
v	venting
0	time at which the flame enters the duct
–	Reynolds average quantity
∼	Favre average quantity

as the occurrence of this flame front instability is well acknowledged even in simply vented vessels [14]. Besides, as pointed out by the same authors, such oscillations should have more pronounced effects on larger scale explosions as confirmed by Kumar et al. [15], who detected severe Helmholtz type oscillations for middle scale lean hydrogen–air explosions vented through a duct.

The turbulent mixing of hot and fresh gases in the initial section of the duct after the flame entrance promotes a violent burning therein (an explosion-like combustion or "burn-up"). Hence, the pressure impulse in the duct induces the backflow of gases from the duct to the vessel with the possible consequent turbulization of residual combustion in the vessel and the blockage of the gas efflux [4,5]. This violent explosion in the duct named as burn-up was addressed by some authors as the main responsible for the dramatic increase of the pressure in the vessel [4,5,9,16].

Other authors indicated additional pressure drops due to the resistance of the gas flow in the vessel–duct assembly as main responsible for the higher pressure rise in the vessel with respect to simply vented vessels [17,18]. Mechanical, steady-state type pressure drops for the present configuration can be substantial due to the very high flow velocities attained in the duct and the concentrated losses in the sudden flow area changes (respectively, at the duct entrance and exit).

On the theoretical side, some efforts have been devoted to get insights into the phenomenon by developing mathematical models. Zero-dimensional models proved effective in advancing the comprehension and the formalization of data gained for simply vented explosions [19–21]. Zero-dimensional and one-dimensional models [4,17] were also proposed to represent an explosion vented through a duct but result in a scarce predictive capability as they rely strongly on empirical parameters. In fact, it could not be expected that such models provided a sound description of the phenomenon due to the assumption of a spherical flame propagation whatever the geometric complicacy (here included the presence of a discharging duct). According to these models the enhancement of the burning rate through tur-

bulization [4] and the friction losses [17] are the most important phenomena affecting overpressure.

The available guidelines for the design of ducted vents for gas explosions are those proposed by Bartknecht [3], also reported in NFPA 68 [1], which gives barely an empirical correlation based on simply vented vessels indications presented in the same reference. Due to their empirical foundation, NFPA correlations are to be used very carefully as they can lead to gross errors [20].

Prior to any correlation development, a sensible approach should be trying to understand the relative contribution of all above reported events to the whole phenomenon. This step appears to be preparatory (if not mandatory) for the selection of the ruling parameters and for the making of the necessary approximations aiming at developing sound engineering correlations.

To this regard it must be noticed that, when care is used in analyzing their results, computational fluid dynamic (CFD) models can be valuable tools in assessing explosion scenarios provided that a satisfactory validation is carried out [22–26]. CFD models can in principle take into account much more physics than zero-dimensional models as they can, for example, relieve the severely restrictive hypothesis on the geometry of the system and of the propagating flame.

In this work a theoretical model for the gas explosion vented through a duct has been developed and numerically solved by means of the CFD-ACE+ code by CFDRC [27]. The model has been validated and tested against the comprehensive set of experimental data of Ponizy and Leyer [5,9]. Comparison of model predictions with experimental data is presented and explanations of experimental observed trends are proposed on the basis of model results. More specifically, the effects of varying the duct geometry (length and diameter) and the ignition position have been studied and analysed with the aid of the numerical computations. Detailed field data gained from the calculations have allowed to evaluate selectively the relative contribution of the mechanical (hindered gas efflux) and chemical (enhanced combustion) contributions to the final pressure load recorded in the system.

2. The model

The analysis of ducted vented explosion has been performed by means of a finite-volume CFD two-dimensional (2D) axis-symmetric model based on the unsteady Reynolds Averaged Navier Stokes (RANS) approach.

2.1. Model equations

The model is based on the following unsteady Reynolds averaged mass, momentum and energy balance equations.

$$\frac{\partial \bar{\rho}}{\partial t} + \frac{\partial}{\partial x_j}(\bar{\rho}\tilde{u}_j) = 0, \quad \text{continuity equation} \tag{1}$$

$$\frac{\partial(\bar{\rho}\tilde{u}_i)}{\partial t} + \frac{\partial}{\partial x_j}(\bar{\rho}\tilde{u}_j\tilde{u}_i) = -\frac{\partial \bar{P}}{\partial x_i} - \frac{\partial}{\partial x_j}(\overline{\rho u_j'' u_i''}),$$

momentum balance equation (2)

$$\frac{\partial(\bar{\rho}\tilde{e})}{\partial t} + \frac{\partial}{\partial x_j}(\bar{\rho}\tilde{u}_j\tilde{e}) = -\bar{P}\frac{\partial \tilde{u}_j}{\partial x_j} - \frac{\partial}{\partial x_j}(\overline{\rho u_j'' e''}),$$

energy balance equation (3)

$$\frac{\partial(\bar{\rho}\tilde{c})}{\partial t} + \frac{\partial}{\partial x_j}(\bar{\rho}\tilde{u}_j\tilde{c}) = \bar{\dot{\omega}}_c - \frac{\partial}{\partial x_j}(\overline{\rho u_j'' c''}),$$

progress variable equation (4)

where ρ, P, u, c, e and $\dot{\omega}_c$ are, respectively, the density, the pressure, the gas velocity, the progress variable, the internal energy and the rate of reaction. The over-bar $(-)$ and symbol $(\sim)$ denote Reynolds and Favre average quantities, respectively, and $(''$) represents fluctuating variables. In order to solve the system of partial differential Eqs. (1)–(4) the averaged flux terms ($\overline{\rho u_j'' u_i''}$, $\overline{\rho u_j'' c''}$, $\overline{\rho u_j'' e''}$) and the mean reaction rate ($\bar{\dot{\omega}}_c$) have to be modelled.

Reliability of RANS predictions strongly depends on reliability of sub-models used to describe the effects of combustion, turbulence and their interactions at the scales not resolved by the numerical grid. In the following the chosen turbulence and combustion models are described.

2.2. The turbulence model

In this work the k–ε model [28] has been used to model the turbulent flow. A number of shortcomings of k–ε models when applied to turbulent combustion problems are known and is generally accepted that more complex second moment Reynolds stress models should be able to describe more of the turbulence–combustion interaction [29]. Nevertheless, at least for the current level of development, the widespread use of second moment models is prevented by their lack of numerical robustness [22], which makes un-worthy their much higher computational cost with respect to traditional two-equations models.

Classical wall functions have been employed for the determination of the flow velocity in the viscous layer adjacent to the walls. To this regard is worth noticing that the use of wall functions is expected to give poor results in the region of flow separation and reattachment, at the duct entrance. Nevertheless, as this region is confined to a very small section at the beginning of the duct, modelling errors related to this choice have been deemed to be not dramatic [30].

2.3. The combustion model

The explosion phenomenon is intrinsically unsteady: starting from ignition in the first vessel, a laminar flame propagates. Due to the turbulence induced by gas expansion and interaction with geometry, in particular with the duct entrance section, transition from laminar flame to turbulent flame may occur trough different combustion regimes.

The starting point in the development of the combustion model was the lack of a universal expression for the averaged source terms valid in all the combustion regimes. To this aim the source term has been adapted at each time step referring to local non-dimensional quantities related to the flow and combus-

tion characteristics (such as the ratio of the turbulent fluctuating velocity to the laminar burning velocity and the Karlovitz number). Different expressions have been used to allow for the different combustion regimes experienced during the explosion:

$$\left(\frac{u'}{S_L}\right) \leq 1, \quad \text{laminar or wrinkled combustion regime} \tag{5}$$

$$\left(\frac{u'}{S_L}\right) > 1 \text{ and } Ka \leq 100, \quad \text{flamelet combustion regime} \tag{6}$$

$$\left(\frac{u'}{S_L}\right) > 1 \text{ and } Ka > 100, \quad \text{distributed reaction zone combustion regime} \tag{7}$$

In the above expressions u' is the root-mean-square (rms) velocity fluctuation defined by $u' = \sqrt{2/3k}$ where k is the turbulent kinetic energy, S_L the laminar burning velocity of the mixture and Ka is the Karlovitz number calculated according to Veynante and Vervisch [31]:

$$Ka = \left(\frac{l_L}{S_L}\right)\left(\frac{\varepsilon}{\nu}\right)^{0.5} \tag{8}$$

where ν and ε are, respectively, the kinematic viscosity and the rate of dissipation of turbulent kinetic energy, and l_L is the laminar flame thickness calculated as:

$$l_L = \frac{\nu}{S_L} \tag{9}$$

The combustion models were implemented in the CFD code by means of user-subroutines. Description of the chosen model for each regime follows.

2.3.1. Laminar flame propagation

A phenomenological approach has been used for the laminar phase propagation [32]:

$$\bar{\dot{\omega}} V_{cell} = Y_u \rho_u S_L A_F \tag{10}$$

where V_{cell} is the volume of the computational cell, Y_u the propane mass fraction in the unburned gases and A_F is the flame area in the computational cell. It is worth noticing that all CFD codes which rely on expressions like Eq. (10) to represent the laminar phase combustion [25,26], involve corrections and/or adjustable parameters to estimate the flame area. In the present work the flame area in each computational cell in the laminar phase has been calculated as:

$$A_F = \xi V_{cell}^{2/3} \tag{11}$$

where the constant ξ (=5/3) has been evaluated by matching the calculated pressure curves in the laminar phase propagation with the experimental trend for a single experimental case and in particular for the rear ignition base test case by [5,9] described in details in Section 3. Any numerical test case or model validation reported in this work has been obtained by using the constant value of ξ reported above.

Table 1
Parameters used for the combustion models, propane–air mixture

α	β	S_l^o (m s^{-1})	C_l	c_1	c_2	g	σ_y
1.77	−0.25	0.42	0.5	2.6	4	1.5	0.5

The acceleration of combustion due to the pre-compression of unburned gases ahead of the flame has been taken into account allowing a dependence of the laminar burning velocity on pressure and temperature:

$$S_L = S_L^o \left(\frac{T}{T^o}\right)^{\alpha} \left(\frac{P}{P^o}\right)^{\beta} \tag{12}$$

where S_L^o is the laminar burning velocity at the reference pressure and temperature P^o and T^o (assumed to be the room conditions), and α and β are constants which vary with fuel. The values of the constants are given for propane in Abu-Orf and Cant [33] and are reported in Table 1.

2.3.2. Flamelet combustion regime

Eddy break up models [34] and algebraic flamelet models [35] have been traditionally the most widely used due to their simplicity and low computational cost. Both these models involve an expression of the type:

$$\bar{\dot{\omega}} \propto \frac{1}{l_T} \tag{13}$$

where l_T is the local integral length of turbulence. Expressions like Eq. (13) lead to not bounded values for the burning rates when combustion spreads near walls as l_T approaches zero near solid surfaces. Due to the particular relevance of combustion into boundary layers in our configuration, a modified form of the algebraic flamelet expression has been used [33]. In this equation the turbulence length is replaced by a laminar length that preserves a finite value close to solid surfaces.

The general algebraic flamelet expression as proposed in Bray and Libby [35] is:

$$\bar{\dot{\omega}} = \rho_u S_L I_o \Sigma \tag{14}$$

where I_o is the "mean stretch factor", assumed as 1 in the present work and Σ is the flame area density expressed as:

$$\Sigma = g\frac{\bar{c}(1-\bar{c})}{\sigma_y L_y} = \frac{g}{\sigma_y L_y}\frac{1+\tau}{(1+\tau\tilde{c})^2}\tilde{c}(1-\tilde{c}) \tag{15}$$

where the constants g and σ_y are, respectively, 1.5 and 0.5, τ the heat release factor ($\tau = T_b/(T_u - 1)$) with T_u and T_b, respectively, the temperature in the unburned and burned gases, and L_y is the characteristic flamelet length expressed in the original version of the model as proportional to the integral turbulence length. In Abu-Orf and Cant [33] the expression for the flamelet length is expressed as a function of the characteristic laminar length and is fitted with an experimentally determined function f which returns the turbulent burning velocity as a function of

the normalized rms velocity (u'/S_L):

$$L_y = C_L l_L f\left(\frac{u'}{S_L}\right) \tag{16}$$

where C_L is a model constant.

Another major issue of this expression is that the empirical function f allows the extension of the validity of the starting expression beyond the flamelet regime to regimes characterized by high strain rates. This characteristic has been of fundamental importance for our configuration as high strain rates and subsequent (temporary) flame quenching are attained in the first sections of the duct [36], thus playing a crucial role in the development of the whole combustion process. It is here important noticing that no adjustable parameter has been fitted in the modified flamelet expression to evaluate the turbulent cell flame area as this value is calculated by the model as a flame area density (Σ).

2.4. Numerical solution

Resolution of the discretized set of Eqs. (1)–(4) has been carried out by means of the SIMPLEC algorithm extended to compressible flows [37]. Pressure-correction methods, extended to allow for arbitrary Mach numbers, are effective in treating the viscous compressible fluid dynamic equations in both the high and low Mach number limits, which both occur in vented explosions.

A fully unstructured grid has been used to mesh the physical domain whose cylindrical shape has allowed the choice of a 2D axi-symmetric numerical domain (see Fig. 1). Non-uniform unstructured grids have been preferred to structured grids aiming at minimizing discretization errors [30] and at avoiding artificial preferential direction of flame [26]. Triangular cells have been used whose characteristic linear dimension (diagonal) lies in the range: $\Delta x = [10^{-3}, 10^{-2}\ \mathrm{m}]$. The smallest cells have been required in correspondence of the vessel–duct restriction while cell size has been relaxed in the bulk of the main chamber and in the external (virtual) chamber the latter being meshed with the coarsest cells. The smallest cells have been required to capture steep gradients characterizing the flow restriction. On the other hand, in the same cells, high flow velocities were attained resulting in critical conditions for the numerical convergence. Hence, our choice has been oriented toward a fully implicit scheme and the fully implicit first order Euler algorithm has then been chosen.

The time step is controlled by a Courant-like criterion:

$$\Delta t_{\mathrm{effective}} = \mathrm{CFL} \times \min(\Delta t_{\mathrm{conv}}, \Delta t_{\mathrm{diff}}, \Delta t_{\mathrm{chem}}) \tag{17}$$

where Δt_i are the characteristic times of the different phenomena in each computational cell (convection, diffusion and reaction) and the CFL parameter is given by the following relationship:

$$\mathrm{CFL} = \frac{1}{\alpha_I} \tag{18}$$

where α_I is the inertial relaxation factor.

The presence of the steep temperature and progress variable gradients at the flame front together with severe gradients of flow velocity and turbulent variables in the boundary layers, has led to the choice of first order upwind differences in the spatial discretization scheme for all the variables in order to avoid numerical instabilities of the computed solutions.

The accuracy of the numerical solutions has been checked by studying three mesh sizes obtained by refining a starting grid: the finer grids have been obtained reducing the cell size of the coarse starting grid (about 12,000 cells). Discretization error has been estimated to be lower than 10% on the finest grid (about 48,000 cells) and about 20% on the coarsest grid (percentage is referred to the estimated exact numerical solution). This difference has been deemed to be not dramatic for the purposes of the present work and all calculations have then been carried out on the intermediate refined grid.

Numerical computations have been carried out on a parallel cluster employing eight processors AMD Opteron 200 (2.4 GHz). Run-times were approximately 6 h for the intermediate grid (24,000 cells).

2.5. Simulation conditions set-up

Validation of the model has been addressed by comparison with the experimental results obtained by Ponizy and Leyer [5]. They reported tests carried out in a cylindrical vessel of fixed volume ($V = 0.0036\ \mathrm{m}^3$) connected to a coaxial cylindrical duct. A sketch of the base case experimental set-up is shown in Fig. 1,

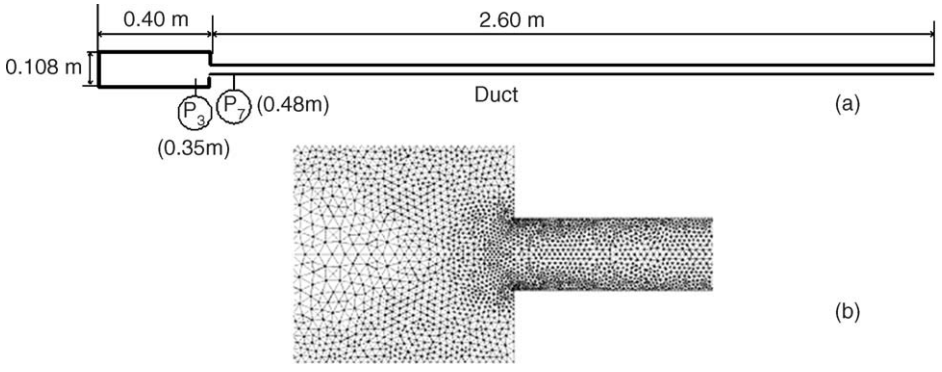

Fig. 1. (a) Experimental set-up of Ponizy and Leyer [4]. The major monitor points are shown. Dimensions are in meters. (b) Non-uniform fully unstructured numerical grid used for simulation. Detail of the duct entrance.

where the experimental monitor points corresponding to numerical monitor points, for the sake of comparison, are also reported.

Experiments were performed for propane–air stoichiometric mixtures ($Y_u = 4.0$ vol.%) and by varying the tube length L_t, the duct diameter D_t and the ignition position (either in the geometrical center of the main vessel or in the rear side, opposite to duct entrance). Initial conditions consisted in atmospheric pressure and temperature for all performed test.

3. Results and discussion

In the following, the model results are compared with the experimental results of Ponizy and Leyer [5,9]. Hence, insights into the phenomena affecting the dramatic increase of pressure in the case of ducted venting are given.

A base case is first defined as the case with tube length $L_t = 2.6$ m and diameter $D_t = 0.036$ m and rear ignition.

For this configuration, Fig. 2 shows the pressure histories in the vessel (monitor 3 in Fig. 1) as obtained by the experiment [5] and by the numerical simulation. For the same case, Table 2 reports the comparison between the peak pressure (P_{max}), the time at which the flame enters the duct (t_0) and the corresponding vessel pressure (P_0), for both numerical and experimental tests.

The experimental pressure trace of Fig. 2 shows that before the flame enters the duct ($t < 39$ ms), a laminar-like flame propagation occurs and that the pressure reaches a quasi-steady-state as the pressure trend seems to reach a plateau: before the flame enters the duct, the combustion rate is balanced by the venting rate. Soon after the flame enters the duct, a steep increase of the pressure occurs and the peak pressure is reached. This qualitative issue featuring the experimental traces has also been captured by the numerical results.

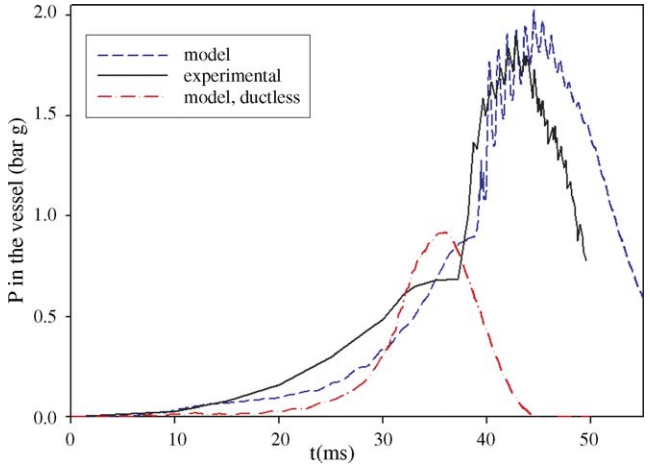

Fig. 2. Pressure at monitor 3 (see Fig. 1, $x = 0.35$ m) as measured experimentally and calculated by CFD simulation. The correspondent pressure history obtained in the absence of duct is also reported.

Table 2
Comparison between the experimental and the calculated values of pressure and arrival time of flame to the duct entrance

	P_{max} (bar g)	P_0 (bar g)	t_0 (ms)	$P_{max} - P_0$ (bar)
Experimental	1.90	0.69	37	1.21
Model	2.02	0.9	39	1.12

Rear ignition; $L_t = 2.6$ m; $D_t = 0.036$ m.

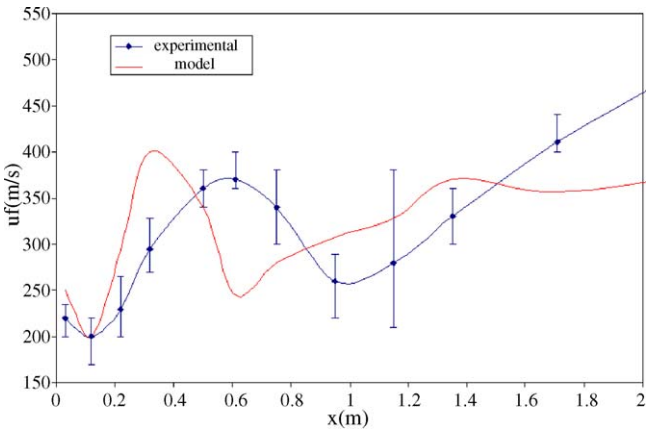

Fig. 3. Flame speed as a function of the axial position in the duct. Experimental and model results for the base test case: $L_t = 2.6$ m, $D_t = 0.036$ m, rear ignition. Flame speed values are referred to a fixed frame of reference (laboratory frame).

Shortly after the flame entrance in the duct, the vessel pressure shows an oscillating behaviour. The computed amplitude (≈30 kPa) and frequency (≈1500 Hz) of the pressure oscillations are close to the experimental values reported by Ponizy and Leyer [5,9]. To this regard, it must be noticed that the fundamental resonant frequency of the cylindrical vessel under consideration is about 1200 Hz [38]. The observed pressure oscillations could then be related to the acoustic modes of the vessel when the flame has already entered the duct leaving an almost completely burned mixture in the combustion chamber.

In Fig. 3, the flame speed relative to a fixed observer (u_F) as a function of the duct axial position is plotted as obtained by the experiments and by simulation of the base case. For both trends two quenching points are found, as the flame speed shows two relative minima.

The first point is observed in a section close to the duct inlet ($x_{duct} \approx 0.1$ m), whereas the second quenching point is found at $x_{duct} \approx 1$ m by the experiments and slightly upstream, $x_{duct} \approx 0.6$ m, by the numerical model. It is here worth noticing that the flame quenching at the beginning of the duct is a key phenomenon in the subsequent development of combustion in the duct. The flow restriction at the duct entrance induces a flow separation zone at the beginning of the duct followed by a reattachment zone where turbulent mixing occurs between cold and hot gases [36]. This fast mixing suddenly withdraws heat from the propagating flame temporarily quenching it but at the same time poses conditions for the subsequent violent local combustion (burn-up).

The agreement between model and experimental results has been deemed to be satisfactory standing the ability of the model to reproduce both the pressure history, a global variable, and, more effectively, the dynamics of flame propagation. Hence, the numerical results have been exploited to assess the effect of different phenomena on the vented explosion.

In Fig. 2, the model pressure trend obtained in the absence of the duct is also reported. The presence of the duct causes a

dramatic increase of the peak pressure from 0.9 to 2.02 bar g, thus approximately doubling the peak pressure.

The reason for the dramatic increase of the pressure has to be clarified. As cited above, Ural [17] and Lunn et al. [18] assumed frictional losses in the vessel–duct assembly as the main mechanism responsible for the increase of the vessel pressure with respect to the corresponding simply vented vessel. Conversely, Ponizy and Leyer [5,9] and Molkov [4] addressed the combustion in the duct (in particular the secondary explosion occurring in the initial sections of the duct). The two hypotheses are discussed and analysed in the following.

3.1. Burn-up related effects

In Fig. 4, for the base case defined previously, the pressure history in the vessel P_3 is compared to the pressure in the initial sections of the duct P_7, and to the pressure difference between the vessel and the duct $\Delta P = P_3 - P_7$ (all computed values). From the figure, it is clear that during the flame propagation in the vessel ($t < 39$ ms) P_3 is higher than P_7, thus promoting the mass flow rate from the vessel to the duct. After the flame enters the duct ($t > 39$ ms), a sharp increase of the pressure in the duct occurs (burn-up) inducing a temporary sign reversal of the pressure difference across the duct entrance (backflow). The plot of the venting rate against time suggests that this inversion is accompanied with an effective flow reversal.

It is known that the peak pressure reached in a vented vessel is the outcome of a competition between the combustion rate and the venting rate that, following Molkov [19], can be formalized as:

$$P_{\max} = \varphi\left(\frac{\text{combustion rate}}{\text{venting rate}}\right) \tag{19}$$

where φ is a function determined by means of a zero-dimensional model.

On this basis, it has to be still understood if the overpressure inside the ducted vessel is the result of the mechanical effects, due to a low effectiveness regime of venting or rather to chemical effects, because the flux *shot* from the duct to the vessel turbulizes the flame and promotes a more intense combustion.

3.1.1. Mechanical effect: venting rate

When burn-up occurs ($t = 39$ ms), the velocity of flow is directed from the duct toward the vessel. In Fig. 4 venting rate and the pressure drop are shown as function of time. The venting rate was calculated according to the following formula:

$$\dot{m}_{\mathrm{v}} = \int_{A_{\mathrm{v}}} \rho u \, \mathrm{d}A_{\mathrm{v}} \tag{20}$$

where $\dot{m}_{\mathrm{v}}$ is the mass flow rate through the vent section, A_{v} the venting section (which corresponds to the duct section) and u is the axial component of velocity. From Fig. 4, it is possible to see the inversion of the flow rate when the duct pressure becomes higher than the vessel pressure ($\Delta P < 0$). When negative venting rate occurs, combustion in the vessel proceeds as in a closed equipment and the pressure increases as burnt products are not vented.

3.1.2. Chemical effect: turbulization

In Fig. 5, the propane mass fraction field is plotted in the vessel–duct configuration before the flame enters the duct ($t = 30$ ms), when the flame enters the duct ($t = 38.4$ ms) and in correspondence of burn-up, i.e. when the pressure in the initial section of the duct ($x = 0.47$ m; monitor 7) reaches a peak value ($t = 39.8$ ms).

At $t = 30$ ms the flame is still in the vessel and the flame propagation is laminar. At $t = 38.4$ ms the flame is just entering the

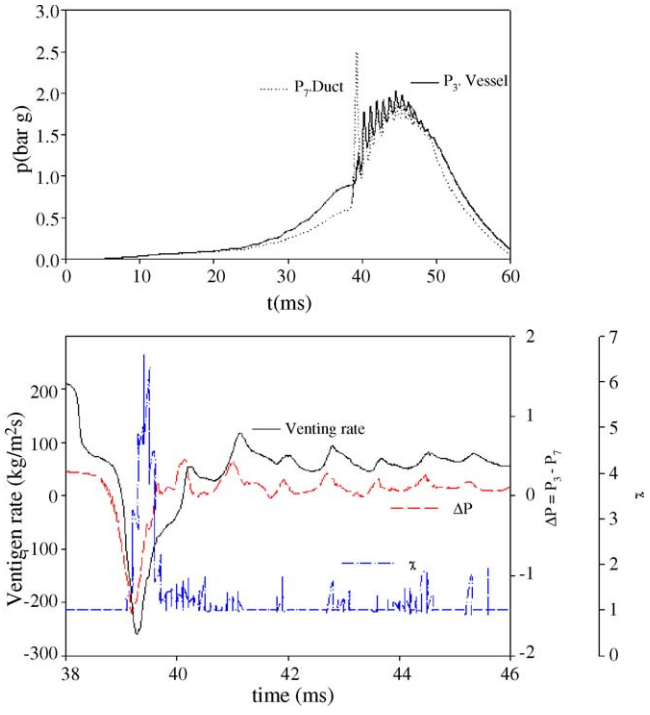

Fig. 4. Vessel (P_3, $x = 0.35$ m) and duct (P_7, $x = 0.47$ m) pressure, venting rate, pressure difference across the duct entrance and turbulization factor in the vessel as a function of time.

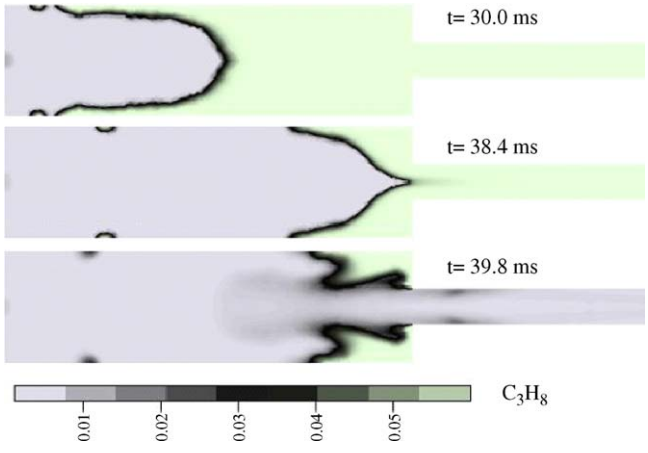

Fig. 5. Propane mass fraction field in the vessel–duct configuration before flame enters the duct ($t = 30$ ms, top), when the flame enters the duct ($t = 38.4$ ms, center) and in correspondence of burn-up ($t = 39.8$, bottom).

duct. The backflow following the burn-up ($t = 39.8$ ms) interacts with the flame in the vessel causing both a flame deformation (grid-resolved) and a turbulence-induced flame wrinkling (subgrid). From this time on the combustion in the vessel proceeds in the flamelet regime and the burning rate experiences an effective increase as a consequence of the overall flame area increase.

In order to quantify the increase of the burning rate taking into account the subgrid increase of the flame surface due to the turbulence, we have evaluated the turbulization factor χ defined in analogy with Molkov [19]:

$$\chi = \frac{\text{turbulence} - \text{wrinkled flame surface}}{\text{smooth flame surface}} \quad (21)$$

In Fig. 4, the value of χ averaged on the whole flame surface is plotted as a function of time together with the pressure drop. It turns out that when backflow occurs ($\Delta P < 0$), χ increases from 1 (laminar flame propagation) to about 7, suggesting that shortly after the burn-up the combustion rate exhibits a great enhancement.

It is here worth noting that the effective pressure rise enhancement depends not only on the burning rate but also on the actual amount of residual unburnt mixture present in the vessel at the moment of back-flow. In Fig. 5, it is shown that at the instant after the burn-up cold unburnt mixture is still present in the vessel.

Model results have been exploited to assess the relative effect of mechanical and chemical phenomenon on pressure rise. Fig. 6 shows the vessel pressure as a function of time in the standard case (RUN 1) and in the simulation performed by eliminating the effect of turbulence on the residual combustion in the vessel (laminar flame). The results obtained for the un-ducted vented vessel (RUN 2) are also reported for the sake of comparison. In this way, we have intended to eliminate the combustion effect (i.e. enhanced burning rate in the vessel due to turbulization) and to take into account only the mechanical effect (i.e. the reduced effectiveness of venting due to combustion in the duct). It is worth noting that in the case of a purely laminar flame propagation in the vessel the peak pressure is slightly lower (1.72 bar g rather than 2.02 bar g) but it is considerably higher than that reached in the corresponding simply vented vessel. This result has allowed us to quantify the relevance of turbulization with respect to the mechanical effect on the final vessel overpressure, suggesting that the mechanical effect (again, here intended as a reduced venting effectiveness due to combustion in the duct) is – at least in the investigated conditions – more relevant than the turbulization effect.

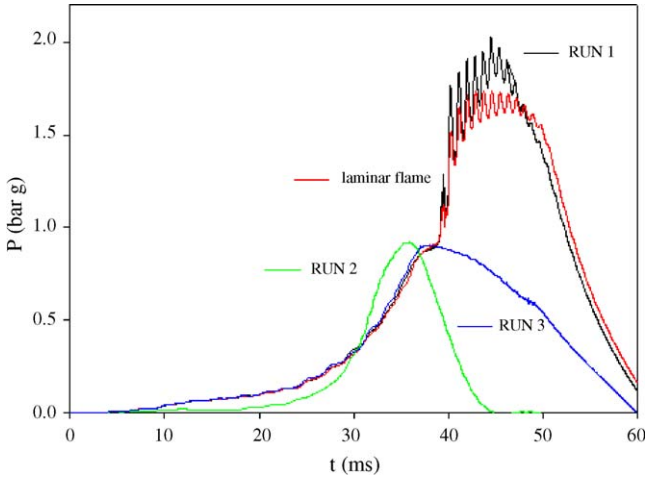

Fig. 6. Calculated pressure histories in the vessel (monitor 3); vessel with duct, base case (RUN1); vessel with duct in the absence of turbulent enhancement of the burning rate in the vessel; vessel without duct (RUN2); vessel with duct in the absence of combustion in the duct (RUN3).

3.2. Gas column inertia and frictional losses

To assess the weight of the gas column inertia and the frictional losses with respect to burn-up on the pressure rise we have run simulations by assuming as zero the source term for reaction rate in the duct, i.e. numerically suppressing the burn-up (RUN3, Fig. 6). We have then compared the results with the standard simulation results and with the simply vented vessel results. In the ductless simulation (RUN 2), the slope of pressure history changes earlier than the other two cases thus suggesting that the flame reaches the vent section earlier with respect to the presence of the duct ($t_0 = 30$ ms instead of $t_0 = 39$ ms). Earlier arrival of the flame at the venting opening brings an earlier start of the disturbing effects related to the venting process and that affects earlier the slope of the pressure trace.

Nevertheless, the flame propagation in the vessel without the duct, before the flame entrance into the duct, induces a lower pressure rise with respect to combustion in the presence of the duct. This difference (≈0.064 bar) could be attributed to the additional frictional losses that arise in the presence of the duct.

More important is noticing that in the absence of reaction in the duct (RUN 3), the peak pressure is significantly lower than that reached in the standard simulation (RUN 1 where combustion in the duct was allowed) and it is almost equal to the simply vented vessel pressure peak (RUN 2).

In conclusion, frictional losses and the gas column inertia have a relevant role in affecting the pressure rise only during the initial laminar flame propagation in the vessel, while combustion in the duct (and more specifically the burn-up related effects as discussed above) seems to be the key mechanism affecting the peak pressure.

This result also confirms the hypothesis of Molkov [4] and Ponizy and Veyssiere [16], who proposed that the peak pressure in this venting configuration could be mitigated by reducing the intensity of combustion in the duct (by means, respectively, of water sprinklers or flame arresters).

3.3. Effects of ignition position

When explosion occurs in simply vented systems, the ignition position strongly affects the peak pressure reached in the vessel. In a very comprehensive review of vented explosion data, Bradley and Mictheson [39] showed that central ignition has to be considered as the worst case (i.e. the one giving the highest maximum pressure) with respect to other ignition positions.

In the presence of venting ducts, Ponizy and Leyer [9] also showed that the vessel overpressure is highest when ignition

Table 3
Effect of ignition position

Ignition	P_{max} (bar g)	P_0 (bar g)	t_0 (ms)	$P_{max} - P_0$ (bar)
Rear				
Experiment	1.76	0.66	33.9	1.1
Model	1.73	0.87	38	0.73
Central				
Experiment	2.01	0.37	22.9	1.64
Model	2.32	0.24	22	2.07

Comparison between the experimental and the model values of pressure and time. $L_t = 1.7$ m and $D_t = 0.036$ m.

occurs at the centre with respect to both the cases of rear and near vent ignition.

Table 3 reports the comparison between the major variables as calculated by the model and experimentally obtained by Ponizy and Leyer [5], for rear and central ignition for a 1.7 m duct length and a 0.036 m diameter.

It is here important noting that even if the rear ignition case is characterized with higher rates of pressure rise in the vessel ($dP/dt_{rear} > dP/dt_{central}$), the final pressure peak is higher in the central case ignition ($P_{max,central} > P_{max,rear}$) and the model is able to follow the experimental trends.

Model results have been employed to assess the hypothesis formulated by Ponizy and Leyer as an explanation of the observed trends.

Ponizy and Leyer [5,9] proposed that in the case of rear ignition most of the unburned mixture is combusted in relatively mild conditions before the burn-up related events (i.e. the backflow and the subsequent turbulization and low effectiveness venting regime). In these conditions, even if the rear ignition case is characterized with higher reactivity after the burn-up (i.e. higher rates of pressure rise in the vessel), a low amount of unburned mixture is available for the residual combustion eventually leading to lower maximum pressure than central ignition.

Plots of Fig. 7 give evidence that the rear ignition case is characterized with a more prolonged, quasi-steady, laminar-like ($\chi = 1$) combustion before the backflow occurs (negative venting rate) and before pressure build up effects commence in the vessel. Moreover, Fig. 7 confirms that a more intense burning rate enhancement is to be expected in the rear case as $\chi_{rear,max} > \chi_{central,max}$. On the other hand, the same figure suggests that the enhanced combustion phase in the rear case is of very short duration while it stands for a quite longer time in the central ignition case. It is just worth noticing that the latter issue is the definite indication of a higher quantity of residual unburned mixture in the vessel in the central ignition case that eventually leads to higher peak pressure.

3.4. Effect of duct length

The effect of the duct length on explosions vented through relief pipes was extensively studied in the literature [3,5–7,40] allowing to establish quite a clear trend. The maximum pressure experiences a very rapid increase with the initial increase of the duct length, while increasing (or even decreasing) with lower rates as the duct length is further increased. Effects related to

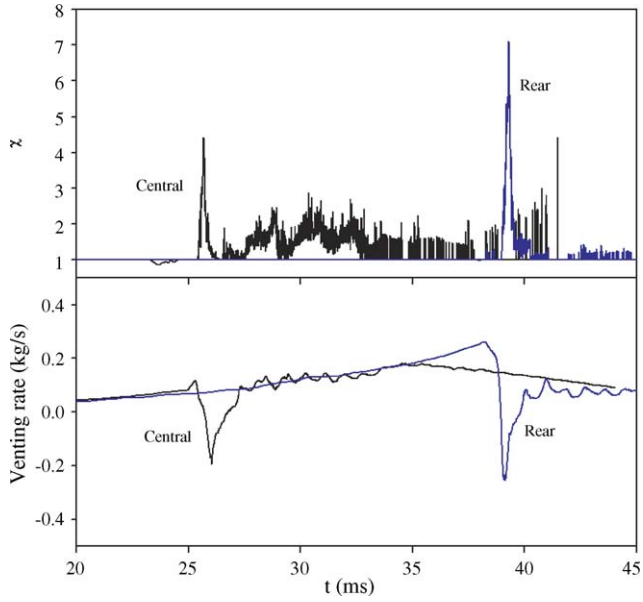

Fig. 7. Effect of ignition position. Comparison between calculated turbulence factors and venting rates for rear and central cases ignition. $L_t = 1.7$ m; $D_t = 0.036$ m.

the duct length were traditionally dealt with guessing a role for the additional pressure drops related to the presence of the duct [3,18]. Indeed, as already mentioned, the flow resistance in the vessel–duct assembly causes a pressure drop that adds to the combustion-related pressure rise in the vessel.

Ponizy and Leyer [5,9] carried out tests varying the duct length between 0.6 and 2.6 m. In Fig. 8, the comparison between

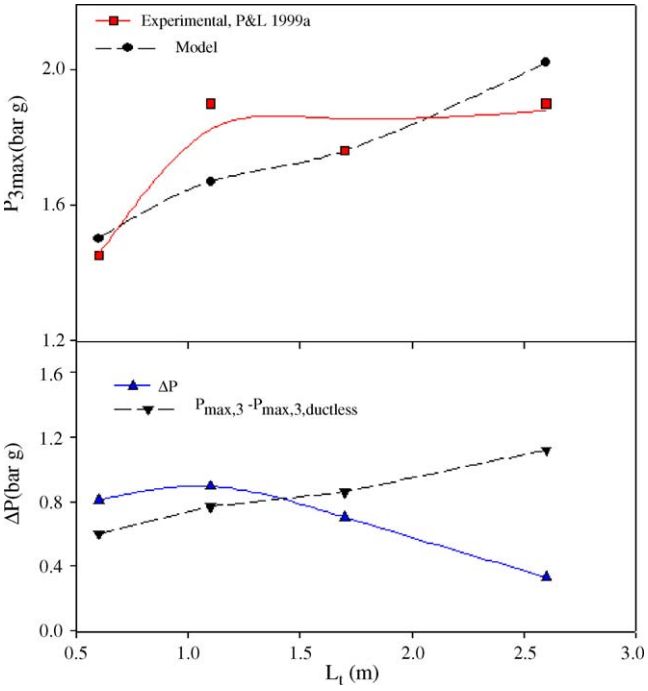

Fig. 8. Duct length effect. Comparison between calculated and experimental maximum pressure in the vessel as a function of duct length; comparison between calculated pressure drops and duct related pressure rise in the vessel ($P_{3,max} - P_{3,max,ductless}$ vs. L_t) following burn-up effects.

model and experimental results for a 0.036 m duct diameter is reported. Both the experimental and the model data show an increasing trend as function of the duct length. Numerical results have been used to gain some insights into the shape of the maximum pressure in the vessel as a function of the duct length trying to ascertain the role of purely mechanical pressure drops. Calculated flow gas velocities (averaged values along the duct axis) have been collected for the various duct lengths aiming at estimating the additional pressure drops due to the presence of the duct. Fig. 8 reports the evaluated pressure drops as a function of the duct length relative to instants following the burn-up. Steady-state pressure drops have been evaluated by means of Eq. (22):

$$\Delta P_{\text{steady}} = \Delta P_{\text{in}} + \Delta P_{\text{duct}} + \Delta P_{\text{out}} = \frac{1}{2}\rho u^2 \left(K_{\text{in}} + 4F\frac{L_{\text{t}}}{D_{\text{t}}} + K_{\text{out}} \right) \quad (22)$$

In Eq. (22), ΔP_{steady} is the overall pressure loss across the duct, ΔP_{in} and ΔP_{out} the concentrated pressure losses at the duct entrance and exit, ΔP_{duct} the distributed pressure loss along the duct, K_{in} and K_{out}, respectively, the pressure loss coefficients for a sudden flow area restriction and a sudden flow area enlargement (compressibility effects have been taken into account using values suggested in Benedict et al. [41]) and F is the friction factor for the flow in the duct evaluated from traditional relationships [42].

In Fig. 8, the pressure drop calculated according to Eq. (22) and the difference between the peak pressure in the vessel in the presence of the duct and that in the corresponding ductless vessel ($P_{3,\text{max}} = 0.9$ bar g) are plotted versus the duct length. It is worth noting that the order of magnitude of these pressure differences is the same suggesting that the effect of length is mainly related to the pressure drop. As a consequence by increasing the duct length, the overpressure in the vessel is increased according to the pressure drop.

3.5. Effect of diameter

The effect of vent area on the maximum pressure reached in a simply vented gas explosion was thoroughly investigated [20,39]. Analysis of very large data collection in such works allowed to derive empirical correlations reporting an always monotonic decrease of the maximum pressure with vent area.

To the authors' knowledge, studies of the vent area effects for gas explosions vented through relief pipes were only performed by Ponizy and Leyer [5,9] and by Molkov [4].

An interesting issue was shown in the paper of Ponizy and Leyer [5] as the vessel overpressure displayed a non-monotonic behaviour with respect to the vent area (i.e. the duct diameter). In particular the maximum pressure was observed to exhibit a minimum in correspondence of an intermediate value of the duct diameter for all the investigated duct lengths.

In the present work, the experimental results of Ponizy and Leyer [5] for a 1.1 m duct length and three duct diameters (0.016, 0.021 and 0.036 m), have been numerically reproduced. As seen in Table 4, the model is able to predict the experimental non-monotonic behaviour. In Fig. 9, the propane mass fraction is shown for the three diameters in correspondence of the backflow time (i.e. when the burning rate enhancement is expected to occur in the vessel).

Table 4
Effect of diameter

Diameter (m)	$P_{3,\text{max}}$ (bar g)	$P_{3,0}$ (bar g)	t_0 (s)
0.016			
Experiment	1.75	1.25	65
Model	2.14	1.67	66.5
0.021			
Experiment	1.4	0.9	51
Model	1.55	1.1	51.3
0.036			
Experiment	1.9	0.6	34.9
Model	1.67	0.71	36.1

Comparison between calculated and experimental values.

Fig. 10 reports the venting rates and the flame averaged enhancement factors (χ) as function of time, for the three diameters. It can be seen from the latter that flame propagation in the vessel vented through the smallest duct diameter is almost un-disturbed with respect to the larger diameters (the χ factor value is definitely lower than the other two). At the same time, even if no substantial combustion enhancement is observed, the venting effectiveness is so low that it prevails in determining the pressure rise.

Therefore, even if venting effectiveness is higher for the highest diameter ($D_{\text{t}} = 0.036$ m), the burning rate enhancement prevails, leading to higher pressure rise, as also hypothesized by Ponizy and Leyer [5] for the observed trend.

The non-monotonic trend can be explained as the outcome of the competition between the burning rate and the venting rate. Increasing the duct diameter is always accompanied with the increase of the venting rate, which tends to relieve the pressure in the vessel. On the other hand, larger diameters result in more pronounced flame distortions, thus promoting the pressure rise

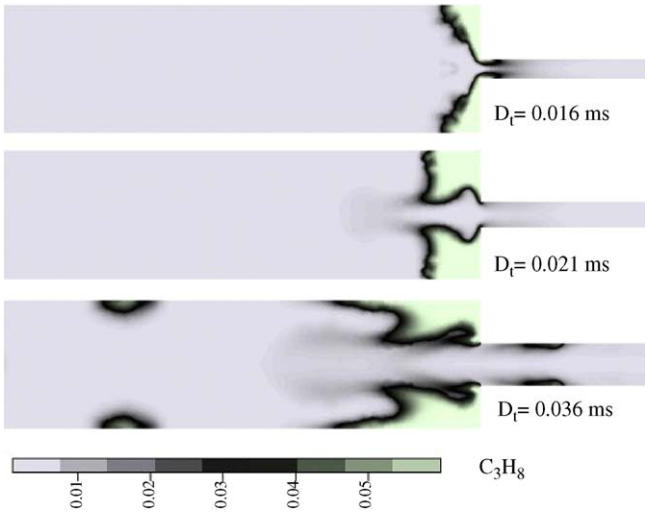

Fig. 9. Effect of diameter. Visualization of the progress variable field after burn-up for different diameters: $D_{\text{t}} = 0.016$ m (top); $D_{\text{t}} = 0.021$ m (central); $D_{\text{t}} = 0.036$ m (bottom). $L_{\text{t}} = 1.1$ m.

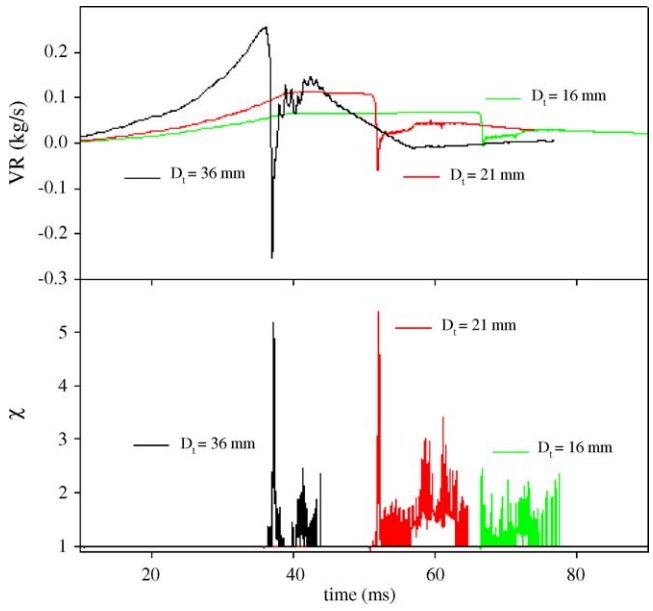

Fig. 10. Effect of diameter. Comparison between calculated venting rates and turbulent enhancement factors for different diameters.

in the vessel. This issue can possibly allow the definition of optimum design for vent sizing, at least at the scale of the reproduced experiments.

4. Model performance evaluation

In order to verify the CFD model used we have applied the test based on MEGGE Protocol by European Community for gas explosion model evaluation [43]. According to this test, it is possible to evaluate the performance of the model by calculating the bias and the variance. We have then represented our model results in comparison with the experimental results of Ponizy and Leyer [5,9] in the mean-variance diagram. The geometric mean (GM) and the variance (σ) have been calculated as follows:

$$\mathrm{GM} = \exp\left(\left\langle \ln\left(\frac{P_{\mathrm{model}}}{P_{\mathrm{exp}}}\right)\right\rangle\right) \tag{23}$$

$$\sigma = \exp\left(\left\langle \ln\left(\frac{P_{\mathrm{model}}}{P_{\mathrm{exp}}}\right)^2\right\rangle\right) \tag{24}$$

where P_{model} and P_{exp} are, respectively, the model value and the experimental value, and the term $\langle x\rangle$ represents the mean expectation value. In Fig. 11, the geometric mean is plotted versus the variance as obtained by averaging the seven simulation results in term of the overpressure reached in the vessel. It is shown that the resulting simulation point (•) lies in the zone where the systematic error of the over or under prediction of the overpressure is absent (GM = 1) and the confidence level (variance) is acceptable.

In the bottom of Fig. 11 the overpressures obtained by the simulations are shown as function of the overpressure obtained in the experiments. It is shown that almost all the results lie in the 50% with a mean relative error equal to 8.6% and a standard deviation of the relative error equal to 13.3%.

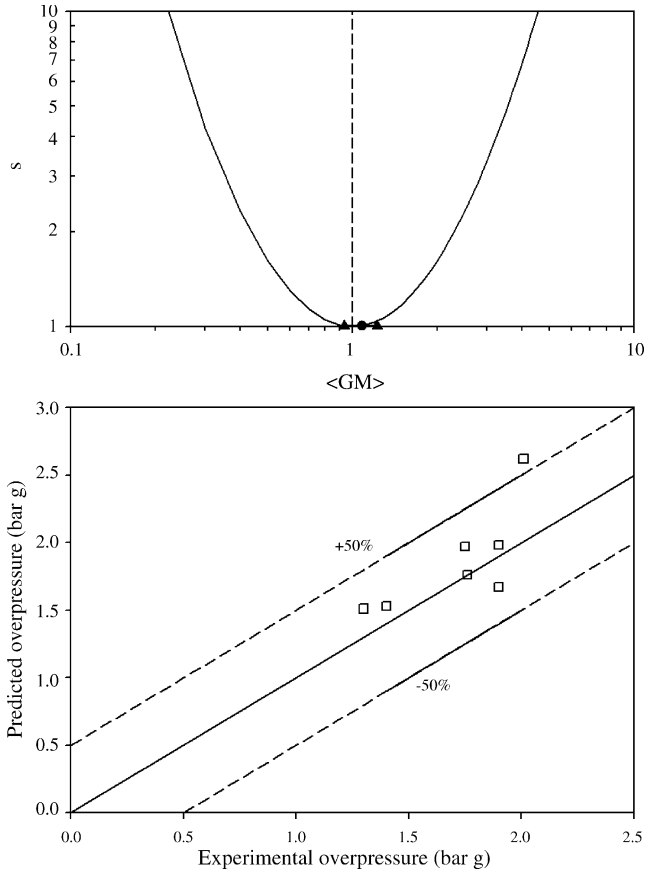

Fig. 11. Model evaluation: geometric mean variance vs. geometric mean bias (top) and predicted vs. experimental overpressure (bottom).

This comparison has been performed for a set of only seven simulations. However, it suggests that the performance of the CFD model with respect to the explosion simulation in such configuration is satisfactory.

5. Conclusions

A CFD model based on the unsteady RANS approach for the numerical simulation of a gas explosion vented through a duct has been proposed.

In this model an adjustable parameter is present for the calculation of the flame area of the laminar combustion rate. This parameter has been identified by matching the computed and the experimental pressure of the rear ignition case. The model has then been validated by comparing the simulation results with the experimental values of peak pressure and flame speeds, keeping fixed this value. The satisfactory agreement between the model results and the experiments has allowed to use the developed CFD code as a numerical tool able to give reliable prediction of the observed experimental trends and it has been then exploited to gain some insights into the phenomenon.

The comparison between simulations of the ductless configuration and by neglecting the source term in the ducted configuration has allowed to ascertain that, the burn-up related effects are the key phenomena in determining the pressure rise in the ducted

venting configuration, in agreement with Ponizy and Leyer, and Molkov findings.

Among the effects of burn-up on the explosion severity it has been shown that the reduction of venting rate (mechanical effect) rather than the burning rate enhancement through turbulization (combustion related effect) is responsible for the recorded overpressure.

Numerical tests have been carried out by varying the duct geometry (diameter and length) and the ignition position. The latter has been found to affect strongly the vessel overpressure through the combustion of the residual unburnt mixture in the vessel after burn-up. With respect to geometrical parameters, numerical flow field representations have indicated that larger duct sections are not a priori beneficial to relieve the pressure in the vessel, due to the flame distortion effects.

References

[1] NFPA 68, Guide for Venting of Deflagrations, National Fire Protection Association, USA, 2002.

[2] R. Siwek, Explosion venting technology, J. Loss Prev. Process Ind. 9 (1996) 81–90.

[3] W. Bartknecht, Explosions, Course Prevention Protection, Springer-Verlag, Berlin, 1981.

[4] V.V. Molkov, Venting of deflagrations: dynamics of the process in systems with a duct and receiver, in: Proceedings of the Fourth International Symposium on Fire Safety Science, Canada, 1994, pp. 1245–1254.

[5] B. Ponizy, J.C. Leyer, Flame dynamics in a vented vessel connected to a duct: 1. Mechanism of vessel–duct interaction, Combust. Flame 116 (1999) 259–271.

[6] B.J. Wiekema, H.J. Pasman, Th.M. Groothuizen, The effect of tubes connected with pressure relief vents, in: Second International Symposium on Loss Prevention and Safety Promotion in the Process Industries, 1977, pp. 223–231.

[7] W. Kordylewski, J. Wach, Influence of ducting on explosion pressure: small scale experiments, Combust. Flame 71 (1988) 51–61.

[8] F. Bouhard, B. Veyssiere, J.C. Leyer, J. Chaineaux, Explosion in a vented vessel connected to a duct, Prog. Astronautics Aeronautics 134 (1991) 85–103.

[9] B. Ponizy, J.C. Leyer, Flame dynamics in a vented vessel connected to a duct: 2. Influence of ignition site, membrane rupture, and turbulence, Combust. Flame 116 (1999) 272–281.

[10] C.J.M. Van Wingerden, J.P. Zeeuwen, On the role of acoustically driven flame instabilities in vented gas explosions and their elimination, Combust. Flame 51 (1983) 109–111.

[11] M.G. Cooper, M. Fairweather, J.P. Tite, On the mechanisms of pressure generation in vented explosions, Combust. Flame 65 (1986) 1–14.

[12] P.A. Cubbage, M.R. Marshall, Pressures generated in combustion chambers by the ignition of air–gas mixtures, IChemE Symp. Ser. 33 (1972) 24–31.

[13] D.P.G. McCann, G.O. Thomas, D.H. Edwards, Gasdynamics of vented explosions Part I: Experimental studies, Combust. Flame 59 (1985) 233–250.

[14] D.M. Solberg, J.A. Pappas, E. Skramstad, Observation of flame instabilities in large scale vented gas explosions, in: Eighteenth Symposium (International) on Combustion, The Combustion Institute, 1981, pp. 1607–1614.

[15] R.K. Kumar, W.A. Dewit, D.R. Greig, Vented explosion of hydrogen/air mixtures in a large volume, Combust. Sci. Technol. 66 (1989) 251–266.

[16] B. Ponizy, B. Veyssiere, Mitigation of explosions in a vented vessel connected to a duct, Combust. Sci. Technol. 158 (2000) 167–182.

[17] E.A. Ural, A simplified method for predicting the effect of ducts connected to explosion vents, J. Loss Prev. Process Ind. 6 (1993) 3–10.

[18] G. Lunn, D. Crowhurst, M. Hey, The effect of vent ducts on the reduced. explosion pressures of vented dust explosions, J. Loss Prev. Process Ind. 1 (1988) 182–196.

[19] V.V. Molkov, Theoretical generalization of international experimental data on vented explosion dynamics, in: Proceedings of the First International Seminar on Fire and Explosion Hazard of Substances and Venting of Deflagrations, Moscow, 1995, pp. 166–181.

[20] V.V. Molkov, R. Dobashi, M. Suzuki, T. Hirano, Venting of deflagrations: hydrocarbon air and hydrogen–air systems, J. Loss Prev. Process Ind. 13 (2000) 397–409.

[21] V.V. Molkov, A.V. Grigorash, R.M. Eber, D.V. Makarov, Vented gaseous deflagrations: modelling of hinged inertial covers, J. Hazard. Mater. A116 (2004) 1–10.

[22] C.J. Lea, H.S. Ledin, A Review of the State-of-the-Art in Gas Explosion Modelling, Health and Safety Laboratory, HSL/02, 2002.

[23] E. Salzano, F.S. Marra, G. Russo, J.H.S. Lee, Numerical simulations of turbulent gas flames in tubes, J. Hazard. Mater. A95 (2002) 233–247.

[24] F. Rigas, S. Sklavounos, Experimentally validated 3-D simulation of shock waves generated by dense explosives in confined complex geometries, J. Hazard. Mater. A121 (2005) 23–30.

[25] N.R. Popat, C.A. Catlin, B.J. Arntzen, R.P. Lindstedt, B.H. Hjertager, T. Solberg, O. Saeter, A.C. Van den Berg, Investigations to improve and assess the accuracy of computational fluid dynamic based explosion models, J. Hazard. Mater. 45 (1996) 1–25.

[26] P. Naamansen, D. Baraldi, B.H. Hjertager, T. Solberg, R.S. Cant, Solution adaptive CFD simulation of premixed flame propagation over various solid obstructions, J. Loss Prev. Process Ind. 15 (2002) 189–197.

[27] CFD-ACE+, CFD Research Corporation, AL, USA, 2005, http://www.cfdrc.com/.

[28] B.E. aunder, D.B. Spalding, Mathematical Models of Turbulence, Academic Press, New York, 1972.

[29] K.N.C. Bray, The challenge of turbulent combustion, in: Twenty-Sixth Symposium (International) on Combustion, The Combustion Institute, 1996, pp. 1–26.

[30] J.H. Ferziger, M. Peric, Computational Methods for Fluid Dynamics, third ed., Springer, 2002.

[31] D. Veynante, L. Vervisch, Turbulent combustion modeling, Prog. Energy Combust. Sci. 28 (2002) 193–266.

[32] O. Saeter, Modelling and simulation of gas explosions in complex geometries, Thesis for the Dr. Ing. Degree, University of Bergen, 1998.

[33] G.M. Abu-Orf, R.S. Cant, A turbulent reaction rate model for premixed turbulent combustion in spark-ignition engines, Combust. Flame 122 (2000) 233–252.

[34] B.F. Magnussen, B.H. Hjertager, On mathematical modelling of turbulent combustion, in: Sixteenth Symposium (International) on Combustion, The Combustion Institute, 1976, pp. 719–727.

[35] K.N.C. Bray, P.A. Libby, Recent developments in the BML model of premixed turbulent combustion, in: P.A. Libby, F.A. Williams (Eds.), Turbulent Reacting Flows, Academic Press, New York, 1994, pp. 115–151.

[36] N. Iida, O. Kawaguchi, S. Takeshi, Premixed flame propagating into a narrow channel at a high speed, Part 1: flame behaviours in the channel, Combust. Flame 60 (1985) 245–255.

[37] J.P. Van Doormal, G.D. Raithby, B.H. Mc Donald, The segregated approach to predicting viscous compressible fluid flows, ASME J. Turbomach. 109 (1987) 268–277.

[38] T. Poinsot, D. Veynante, Theoretical and Numerical Combustion, R.T. Edwards, 2001.

[39] D. Bradley, A. Mitcheson, The venting of gaseous explosions in spherical vessels. I—theory, Combust. Flame 32 (1978) 221–236.

[40] F.P. Lees, Loss Prevention in the Process Industries, Hazard Identification, Assessment and Control, vol. 2, Butterworth Heinemann, 1996.

[41] R.P. Benedict, N.A. Carlucci, S.D. Swetz, Flow losses in abrupt enlargements and contractions, J. Eng. Power, Trans. ASME 88 (1966) 73–81.

[42] M.M. Denn, Process Fluid Mechanics, Prentice-Hall, 1980.

[43] MEGGE, Model Evaluation Group for Gas Explosion, Gas Explosion Model Evaluation Protocol, European Community, 1997.